Room-temperature creep of $LaCoO_3$-based perovskites: Equilibrium strain under compression

Mykola Lugovy,[1,2] Viktor Slyunyayev,[1] Nina Orlovskaya,[2] Dmytro Verbylo,[1,3] and Michael J. Reece[3]
[1]*Institute for Problems of Materials Science, 3 Krzhizhanovskii Street, Kiev-142, 03142, Ukraine*
[2]*University of Central Florida, Department of Mechanical, Materials and Aerospace Engineering, 4000 Central Florida Boulevard, Orlando, Florida 32816, USA*
[3]*Queen Mary University of London, Centre for Materials Research, School of Engineering and Materials Science, Mile End Road, London E1 4NS, United Kingdom*

(Received 14 February 2008; revised manuscript received 20 April 2008; published 10 July 2008)

This study concerns an experimental investigation of room-temperature creep at different stresses in polycrystalline $LaCoO_3$-based oxides under compression. A phenomenological approach for ferroelastic creep is proposed to identify the most important parameters that affect creep strain over different time periods. An analytical expression is obtained instead of the previously used power law, allowing an estimation of equilibrium strain at constant stress. An expression is also proposed to calculate the characteristic time of creep and recovery processes. The equilibrium creep diagrams for $LaCoO_3$ and $La_{0.8}Ca_{0.2}CoO_3$ perovskites have been determined.

DOI: 10.1103/PhysRevB.78.024107 PACS number(s): 62.20.Hg

I. INTRODUCTION

Mixed ionic-electronic conducting (MIEC) lanthanum cobaltite perovskite-type oxides are well known materials for solid-oxide fuel cells, oxygen separation membranes, catalysts, and oxygen sensors.[1–8] Their high-temperature properties, such as electronic-ionic conductivity, electrochemical performance, and catalytic activity, have been studied to a great extent,[9–12] while the mechanical behavior of the MIEC perovskites is still not completely understood. Recently, the ferroelastic behavior of ferrites and cobaltites has been reported.[13–15] A schematic presentation of the stress-strain diagram of a ferroelastic material is shown in Fig. 1. An important feature that ferroelastic oxides exhibits is room-temperature creep.[16] However, experimental studies of the time-dependent behavior of ferroelastic perovskites are still very rare. The high-temperature creep of selected ferrites and cobaltites has been studied,[17–19] while information on room-temperature creep is restricted to ferroelectric lead zirconate titanate (PZT).[20,21] The room-temperature creep of $LaCoO_3$-based perovskites has not been studied.

Creep is the continuous deformation of a solid with time, and it is traditionally reported to occur at temperatures higher than $0.5T_m$ (T_m is the melting temperature of material). Creep strain is a function of stress, time, temperature, grain size and shape, microstructure, defect mobility, and other material parameters.[22] The high-temperature-creep diagram can be divided into three different stages of creep: primary; secondary; and tertiary creep—each with its own characteristic strain-versus-time behavior [Fig. 2(a)]. The materials' strain at high temperature will continue to increase if the stress is held constant. Initially, the strain rate slows with increasing strain. This is known as the primary creep. The strain rate eventually reaches a minimum and becomes near constant. This is known as secondary or steady-state creep. In tertiary creep, the strain-rate increases exponentially with strain up to the fracture of the material. In ferroelastic ceramics, the room-temperature creep is characterized by an ever decreasing slope of the creep curve [Fig. 2(b)], which most closely resembles the primary high-temperature creep. However, the high-temperature primary creep is followed by a constant nonzero strain-rate stage and further by tertiary creep with failure at the end, while ferroelastic creep, as it was found in the present work, results in an equilibrium saturation strain and zero-strain rate at a given stress [Fig. 2(b)]. Therefore, ferroelastic creep attributed to ferroelastic domain switching requires a different phenomenological approach than the creep of metals.

Strain recovery occurs during the unloading of ferroelastic materials and the strain rate gradually decreases or disappears if the stress is held constant [Fig. 2(c)]. The recovery strain is the difference between the instantaneous strain at the beginning of the constant stress stage during unloading and the actual strain at any time. Both ferroelastic creep and strain recovery have the same mechanism—domain switching—responsible for their occurrence in ferroelastic oxides at room temperature; however the driving forces for these phenomena are different.[23] While creep is induced by applied stress, recovery strain results from residual stresses in ferroelastic domains.

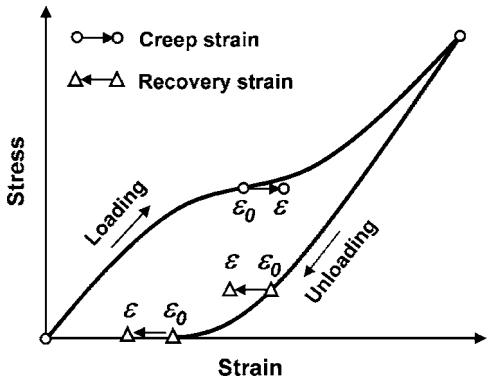

FIG. 1. A schematic representation of a stress-strain diagram for a ferroelastic material. The locations of the instantaneous strain ε_0 and creep/recovery strain ε are shown both during loading and during unloading.

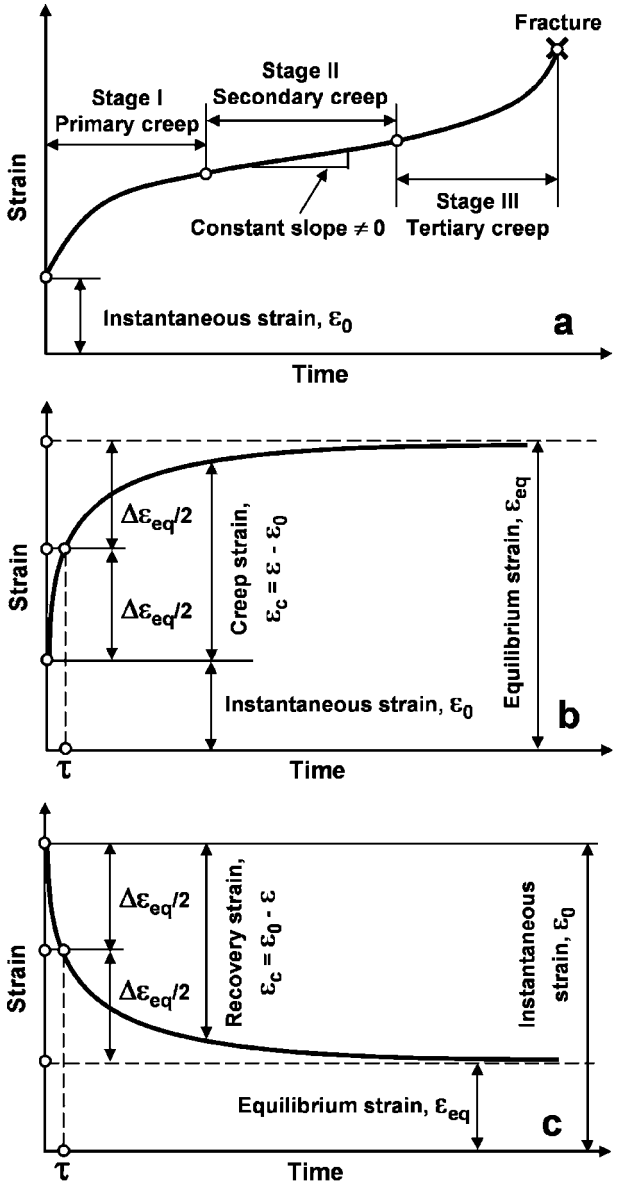

FIG. 2. A schematic representation of high-temperature creep in metals (a), everlasting creep (b), and recovery (c) in ferroelastic materials at room temperature.

Forrester and Kisi[16] investigated ferroelastic switching in poled and unpoled soft PZT material subjected to compressive stresses from 10 to 60 MPa at room temperature. They found that the creep rate decreased with time, indicating a saturation or exhaustive process, and is strongly dependent on the applied stress. A power law was used to fit the creep strain-time dependence at constant stress. Fett and Thun[20] studied the creep behavior of a soft PZT under tensile stress loading. They found that the creep was of the primary type and could be described by a power law. The results found for PZT were similar to those reported earlier by Subbarao *et al.*[24] for polycrystalline barium titanate. Zhou and Kamlah[21] investigated the creep of PZT piezoceramics both under electric field and compressive loading at room temperature. They also found that the creep was of a primary type and could be expressed by an empirical power law with the maximum creep rate occurring at a loading level near the coercive field and coercive stress for initially unpoled samples. These authors considered that the creep mechanism is locally consumable and the total amount of domain switching induced during a constant load is limited. Guillon *et al.*[25] conducted similar compressive creep tests on poled and unpoled soft PZT at two different temperatures. They modeled the observed creep strain rate using a power-law dependence on stress with kinematic hardening. The resulting viscoplastic phenomenological model captured the observed behavior only qualitatively.

The goal of this research was to investigate the room-temperature creep at different stresses in polycrystalline $LaCoO_3$-based perovskites under compression. An attempt has been made to identify the most important parameters that influence creep strain over different time periods. The goal was also to develop an appropriate analytical expression that could substitute the previously used power law, allowing an estimation of equilibrium strain at constant stress.

II. EXPERIMENT

$LaCoO_3$ (LC) and $La_{0.8}Ca_{0.2}CoO_3$ (LCC) perovskites were produced by Praxair Surface Technologies, Specialty Ceramics. The oxides were sintered at 1450 °C for 2 h, and had a porosity of 6%–7%. Pure single perovskite phase with no detectable secondary phases was determined by x-ray diffraction (XRD) for both compositions. An average grain size of 2–5 μm was measured for both compositions. The detailed description of the materials' structures is given elsewhere.[15,26] Cylinders with diameter ≈5.9 mm and height of 12 mm were cut and machined from the sintered samples. The compressive strength of the samples was measured to be 1100 ± 60 MPa.

Compression tests were performed in a servohydraulic test machine (Instron 8511) with a 20-kN load cell. The compression load was applied along the height of the cylinders. Samples were compressed in air at room temperature in loading control mode with a loading/unloading rate of 3 MPa/s. Both monotonic and step loading was performed. The monotonic loading was applied up to 663 MPa followed by full unloading. Stress-strain diagrams recorded during monotonic tests were used to determine the inflection points of the perovskites. A step loading was also performed, and the scheme of the loading/unloading steps is presented in Fig. 3. For this experiment the load was instantaneously applied up to a certain defined load, at which it was held constant for a certain period of time. Smaller stress increments at the beginning of step-loading tests were chosen in order to provide more detail about the material behavior below the inflection point. Similarly, smaller stress increments were used at the beginning of the unloading part in order to provide more detail in this stress range. The hold times at the constant stress were different for LC (120 s) and LCC (180 s) oxides, but were kept constant at the different stress levels. The axial strain was measured using three strain gauges mounted on the surface of each sample. Total strain was determined by averaging the signals from the three strain gauges.

The LCC oxide was also tested for a much longer period of time, where the samples were loaded to 132 MPa and held

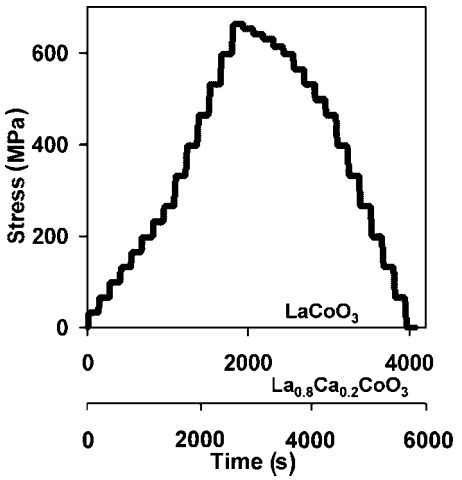

FIG. 3. Stress-time diagram showing the loading history during a uniaxial compression test.

for 419 136 s at constant stress. When changing the stress a loading/unloading rate of 3 MPa/s was used for these experiments performed at RT in air.

III. RESULTS

A. Effect of the step loading on stress-strain diagram and creep strain

It is reasonable to expect that the loading history of a sample will influence the creep strain and other creep parameters. For identical samples loaded to the same constant stress, the instantaneous strain ε_0 could reach different values if the loading rate was different (for example fast and slow loading), or if the steps between the constant stress levels were too short for the strain to be able to recover to the original position on the stress-strain diagram. In this case, as a result of the different ε_0, the creep strain values would also be different. However, if the experiment could be designed in a way that the loading history, such as a step loading (Fig. 3), had a negligibly small effect on ε_0 at a certain stress, then one could expect that the creep strain measured at the consecutively higher stress levels would be almost unaffected by loading history.

In order to verify the effect of loading/unloading steps at constant stress on the stress-strain diagrams and creep strain and, therefore, to validate the proposed experimental approach, two simple experiments have been performed. In the first experiment the stress-strain diagrams have been generated using two different LCC samples. One sample was loaded/unloaded with a maximum stress of 660 MPa without any stress dwells. The other sample had a step loading as presented in Fig. 3. The stress-strain diagrams for these two tests are presented in Fig. 4(a). As can be seen, there is a very good coincidence of the two deformation curves. For the sample deformed with a step loading, the stress-strain curve after dwelling at a certain constant stress tends to achieve the same stress level as the sample deformed without dwells to the same strain as the experiment continues and stress starts rising again. Thus, we can assume that the previous loading/unloading steps on the deformation curve have minimal effect on the creep strain measured under a specific loading rate and at a specific stress level.

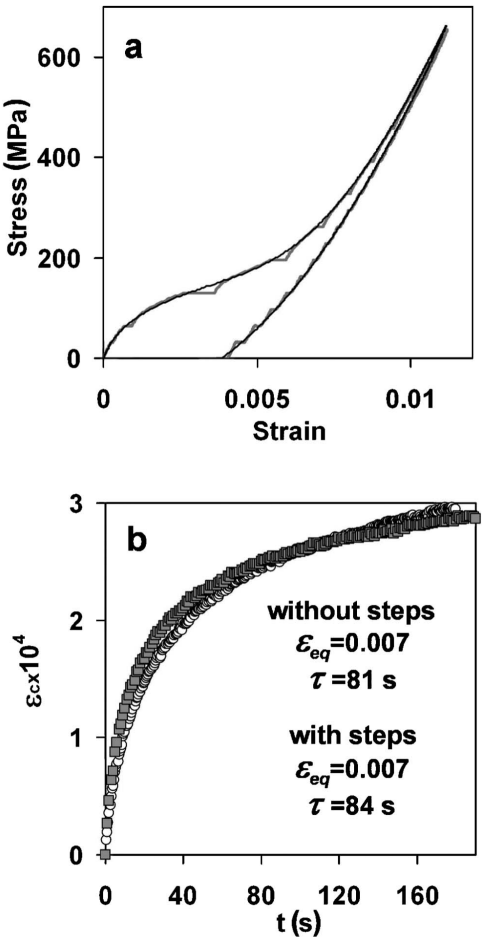

FIG. 4. (a) Comparison of stress-strain diagrams of LCC perovskite. Thin black line is the single loading/unloading deformation diagram up to 660 MPa maximum stress, while thick gray line is the deformation diagram obtained using the loading/unloading scheme presented in Fig. 3. (b) Creep strain versus time plots. One of the plots (○) shows the creep strain recorded at 229 MPa after the step loading, following the loading scheme presented in Fig. 3. Another plot (■) shows the creep strain recorded after a single loading to 229 MPa. The calculated equilibrium strain ε_{eq} and the characteristic time τ were equal to $\varepsilon_{eq}=0.007$ and $\tau=84$ s for the data collected with loading steps (○), and $\varepsilon_{eq}=0.007$ and $\tau=81$ s for the data collected without loading steps (■).

To further verify this conclusion, a separate experiment was performed in which a pristine LCC sample was loaded straight to the stress of 229 MPa and dwelled at this stress level for 200 s. The measured creep strain was then compared to the creep strain for a sample with a loading-step history (Fig. 3) to 229 MPa. The Fig. 4(b) shows the comparison of creep strains as a function of time calculated using these two separate experiments. There is a good coincidence of the results; therefore, we can conclude that the creep strain is similar for materials with or without a step-loading history in our experiment.

B. Ferroelastic creep and strain recovery

Representative strain-time curves for both LC and LCC oxides are shown in Figs. 5(a) and 5(b) and Figs. 5(c) and 5(d), respectively. The creep strains for pure LC perovskites are typically much smaller than the creep strains for LCC perovskites. However, the trends in creep behavior as a function of applied stress are similar for both materials in a short time interval up to 180 s. As the constant applied stress is increased from lower values up to the stress corresponding to the inflection point of the loading curve,[14] the creep strain increases significantly. The coercive stress for LC is 66 MPa as measured by the inflection point of the stress-strain curve of LC. For LC oxide the creep strain at 33 MPa after 120 s hold time is equal to $3.3\cdot10^{-5}$ and $8.14\cdot10^{-5}$ after 120 s at 66 MPa [Fig. 6(a)]. For LCC the corresponding values of creep strain are an order of magnitude higher than those of pure LC. The creep strain at 65 MPa after 120 s is equal to $2.47\cdot10^{-4}$ and $9.2\cdot10^{-4}$ after 120 s at 130 MPa, which is the coercive stress for LCC oxide [Fig. 6(b)]. Upon further increase in the constant stress, for example 198 MPa for LC or 393 MPa for LCC, the creep strain values decrease to $2.63\cdot10^{-5}$ and $1.17\cdot10^{-4}$ after a hold time of 120 s, respectively. For higher values of the constant stress such as 663 MPa for LC and 656 MPa for LCC, the creep strains become very small ($<4\cdot10^{-5}$).

While the creep strain has the highest values at a constant stress equal to the coercive stress of the ferroelastic material upon loading, the recovery strain upon unloading of the ferroelastic oxide constantly increases upon decreasing of the constant stress. Thus, at high constant stresses of 652 MPa for LC and 639 MPa for LCC, the recovery strain is negligibly small. When the constant stress decreases to 132 MPa for LC and 196 MPa for LCC, the recovery strain starts increasing, reaching a maximum values when the constant stress is 0 MPa. The dependence of the recovery strain after 120 s hold time is shown in Fig. 6.

C. Phenomenological expression for creep strain and equilibrium strain

One way of presenting the experimental data for a creep strain-time dependence plot at constant stress is by using logarithmic coordinates. The data obtained for LC and LCC perovskites are presented in Fig. 7. For comparison, the experimental points obtained for PZT materials[20,21] are also presented. In order to predict the long-term time-dependent behavior of the ferroelastic material, the experimental data could be fitted using a power law.[21] As can see from Fig. 7, the best fitting by power law exists for intermediate times of the creep experiments. In contrast, at the beginning and at the longer times deviations from power law are observed. Such deviations during long time experiments appear because of a limited total amount of domain switching induced during a constant applied stress, i.e., exhaustion. The saturation strain can be considered as some equilibrium strain for a given stress. Thus, the power law is not applicable for the description of creep behavior over longer time intervals, since this law allows for an infinite growth of strain and therefore cannot describe the saturation phenomenon prop-

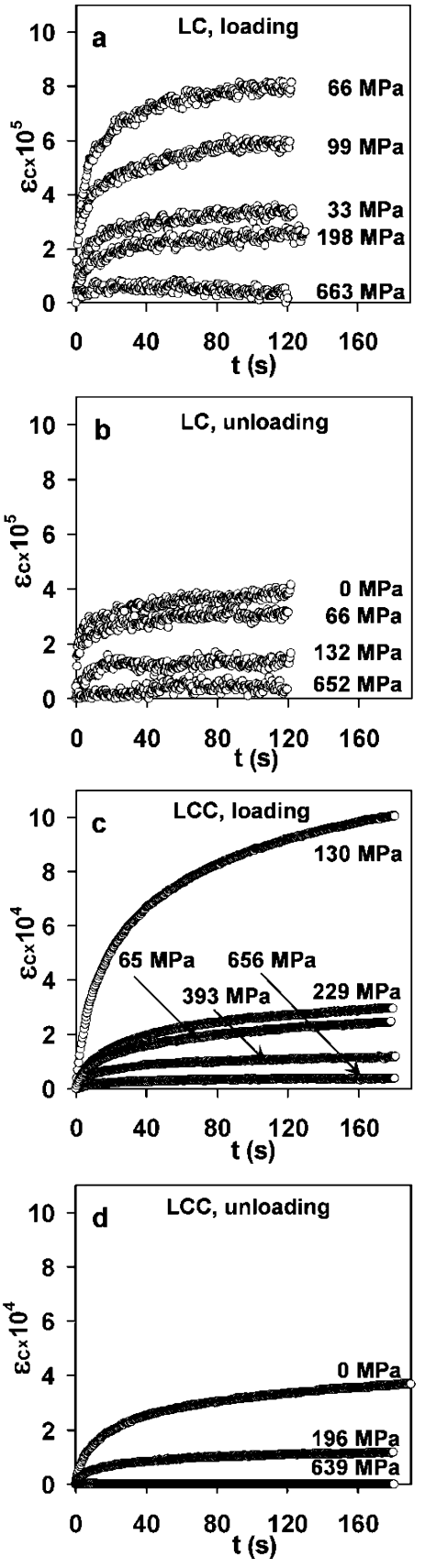

FIG. 5. Creep/recovery strain-time dependence at constant stress for LC [(a),(b)] and LCC [(c),(d)]: (a),(c)—loading; (b),(d)—unloading.

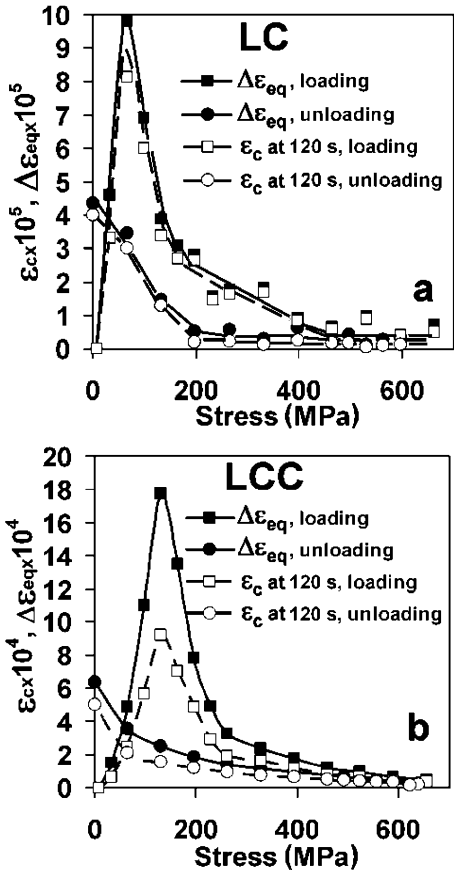

FIG. 6. Dependence of creep/recovery strain after 120 s hold time (dashed line) and estimated equilibrium strain (solid line) as a function of a constant stress: (a) LC (b) LCC.

erly. Therefore, the power law is valid for fitting only over a limited time interval, and a systematic deviation of the experimental creep strain is observed for testing over either very short or very long period of time. These considerations brought us to the fact that other expressions should be developed, which would take into account the existence of finite equilibrium strain at constant applied stress.

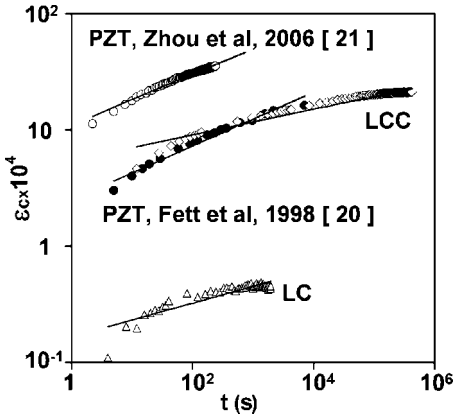

FIG. 7. A creep strain-time dependence at a constant stress presented with a logarithmic scale: (1) Fett *et al.* (Ref. 20), 21.3 MPa; (2) Zhou *et al.* (Ref. 21), 50 MPa; (3) LC, 68 MPa; (4) LCC, 132 MPa, long test; Solid lines correspond to the best fit by a power law.

If we present the creep strain-time dependence as

$$\varepsilon_c = \Delta\varepsilon_{eq} f(t), \tag{1}$$

then we define $\varepsilon_c = |\varepsilon - \varepsilon_0|$ as the creep (or recovery) strain and $\Delta\varepsilon_{eq} = |\varepsilon_{eq} - \varepsilon_0|$ as the equilibrium strain increment, where ε is the total strain (Fig. 1). Further, we define ε_0 as the instantaneous strain at the beginning of constant stress stage (Fig. 1), $\varepsilon_{eq} = \varepsilon_{eq}(\sigma)$ as the equilibrium (or saturation) strain at constant stress σ [Figs. 2(b) and 2(c)], t as the time starting from the beginning of the constant stress stage, and $f(t)$ as the dimensionless monotonic function of time, where $f(t)=0$ at $t=0$ and $f(t)$ approaches 1 when t approaches infinity. This implies that ε will approach ε_{eq} when $t \to \infty$. For convenience, both creep strain and recovery strain are designated as ε_c.

Since a power law demonstrated a good fit for data collected in the 50–300 s time interval (Fig. 7), we will incorporate it into the new function. The simplest way is to consider a new dimensionless variable $z = at^n$, where n is an exponent $(n < 1)$ and $a = 1/\tau^n$, where τ is a characteristic time. Then, the new function is presented as

$$\varepsilon_c = \Delta\varepsilon_{eq} g(z), \tag{2}$$

where $g(z)=0$ when $z=0$ and $g(z)$ approaches 1 when $z \to \infty$ since $z=0$ when $t=0$ and $z \to \infty$ when $t \to \infty$.

One of the simplest functions that meet these conditions is

$$g(z) = \frac{z}{1+z}, \tag{3}$$

so

$$f(t) = \frac{at^n}{1+at^n} = \frac{(t/\tau)^n}{1+(t/\tau)^n}. \tag{4}$$

The parameters ε_{eq}, τ, and n for a given stress can be determined from creep strain (recovery strain)-time diagram [Figs. 2(b) and 2(c)]. While parameters ε_{eq} and τ are different for different stress levels, $n=0.5$ in all cases. In the case where $n=0.5$, the best fit was achieved for LC and LCC oxides. Therefore,

$$\frac{\varepsilon_c}{\Delta\varepsilon_{eq}} = \frac{\tilde{t}^{0.5}}{1+\tilde{t}^{0.5}}, \tag{5}$$

where $\varepsilon_c/\Delta\varepsilon_{eq}$ is the normalized creep strain and $\tilde{t} = t/\tau$ is the normalized time. When $t=\tau$, $\varepsilon_c = \Delta\varepsilon_{eq}/2$, or half of the equilibrium strain increment.

In order to verify the compatibility of the proposed function for the phenomenological description of creep and strain recovery, the normalized creep strain and normalized recovery strain as a function of normalized time at constant stresses have been analyzed (Fig. 8). LC and LCC, as well as PZT[20,21] data, show an excellent correlation with each other both for the loading and unloading portion of the deformation curves. Expression (5) provides an excellent fit for the experimental data.

R^2 fitting parameter has been used for the determination of how good the proposed fit is, since it shows the relative predictive power of a model. R^2 is the fraction of the total squared error and is presented as

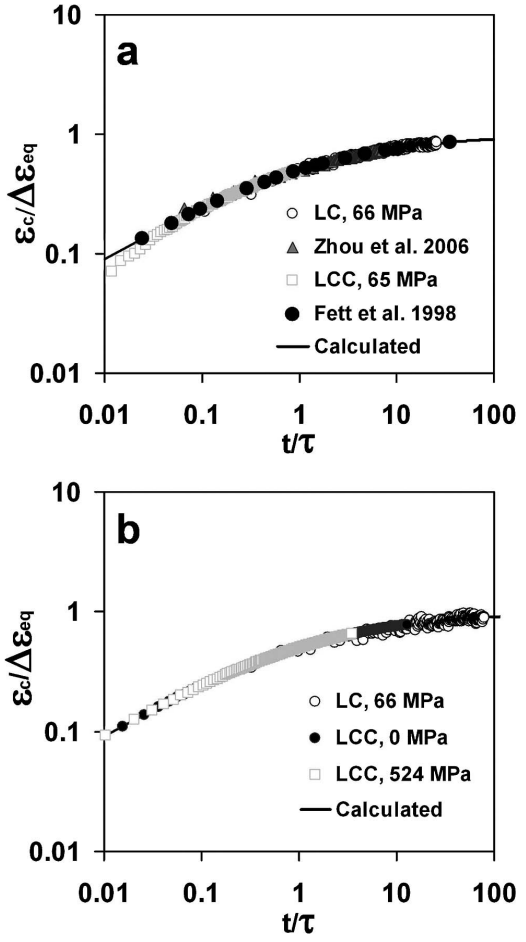

FIG. 8. Dependence of the normalized creep/recovery strain with normalized time at a constant stress: (a) loading stage (b) unloading stage.

$$R^2 = 1 - \frac{\sum_{i=1}^{n} (\varepsilon_i^{(ex)} - \varepsilon_i^{(th)})^2}{\sum_{i=1}^{n} \varepsilon_i^{(ex)^2} - \frac{(\sum_{i=1}^{n} \varepsilon_i^{(ex)})^2}{n}}, \quad (6)$$

where $\varepsilon_i^{(ex)}$ is the experimental value of creep strain corresponding to time t_i, $\varepsilon_i^{(th)}$ is the creep strain calculated using a power law or expression (5) for time t_i, n is the total number of points taken for calculation. R^2 lies between 0 and 1 and if an R^2 value is equal to one, this would imply that the model provides a perfect prediction.

Data collected for LCC perovskites with a hold time of five days (419 136 s) were used to check the fit determination. The R^2 value was calculated using data with different data sets, such that all of the data started from the beginning of constant stress and ended at 180 s or at 419 136 s (5 days). The R^2 parameter for the experimental time of 180 s is equal to 0.975 as calculated by using a power-law fitting and 0.997 using our proposed function. For the long time experiments the R^2 corresponding values are 0.923 using a power-law fitting and 0.977 using the proposed model. During longer creep experiments, when the creep strain is approaching $\Delta\varepsilon_{eq}$, the proposed expression has a greater predictive power of the creep behavior at room temperature. This improved accuracy is simply attributed to its ability to predict what the saturation/equilibrium strains are.

D. Equilibrium strain increment

Another important calculated parameter, equilibrium strain increment $\Delta\varepsilon_{eq}$, demonstrates a similar dependence on applied stress as creep strain at 120 s (Fig. 6). As one can see from Fig. 6(a), the creep strain ε_c measured at 120 s hold time and calculated values of equilibrium strain increment $\Delta\varepsilon_{eq}$ nearly coincide both for the loading and for the unloading portions of the deformation curves for LC. A good coincidence between ε_c and $\Delta\varepsilon_{eq}$ occurs at 65 MPa constant stress, which corresponds to the coercive stress (inflection point) of LC and shows the maximum creep strain. The good correspondence between measured ε_c and calculated $\Delta\varepsilon_{eq}$ means that within 120 s of the hold time at a certain constant stress, the strain of LC perovskite almost reaches the values of the equilibrium strain. At the same time, as one can see from Fig. 6(b), the creep strain ε_c measured at 120 s hold time is almost half of $\Delta\varepsilon_{eq}$ for LCC perovskite at 130 MPa, which means that the creep process or domain switching is much slower, and much more time is required to reach the equilibrium strain. The largest difference between ε_c and $\Delta\varepsilon_{eq}$ is obtained at the 130 MPa constant stress, which corresponds to the coercive stress (inflection point) of LCC.

$\Delta\varepsilon_{eq}$ can be considered as a measure of the number of domains available for switching at a given applied stress. It reaches a maximum at the coercive stress (inflection point) of the ferroelastic material during loading, which means that at the inflection point the largest number of domains is available for switching. For the unloading the $\Delta\varepsilon_{eq}$ monotonically increases as stress is decreasing with the largest $\Delta\varepsilon_{eq}$ value corresponding to zero applied stress, i.e., maximum switching stress increment.

E. The characteristic time and switching stress increment

In addition to the equilibrium strain and the equilibrium strain increment, another important room-temperature creep parameter is the characteristic time τ, which is the time required to reach a strain located half way between the instantaneous and equilibrium strain at some constant stress [Figs. 2(b) and 2(c)]. The characteristic time is to be used for the evaluation of how fast ferroelastic creep or strain recovery will occur in a ferroelastic material, and it shows that the ferroelastic creep and strain recovery will be faster for the material with a smaller characteristic time given that the instantaneous strain and equilibrium strain values are the same for the materials under consideration.

The mechanisms responsible for the room-temperature creep, such as, for example, domain switching, determine the characteristic time, which obviously depends on the switching rate. We define a new parameter, the switching stress increment $\Delta\sigma$, which determines switching rate, as

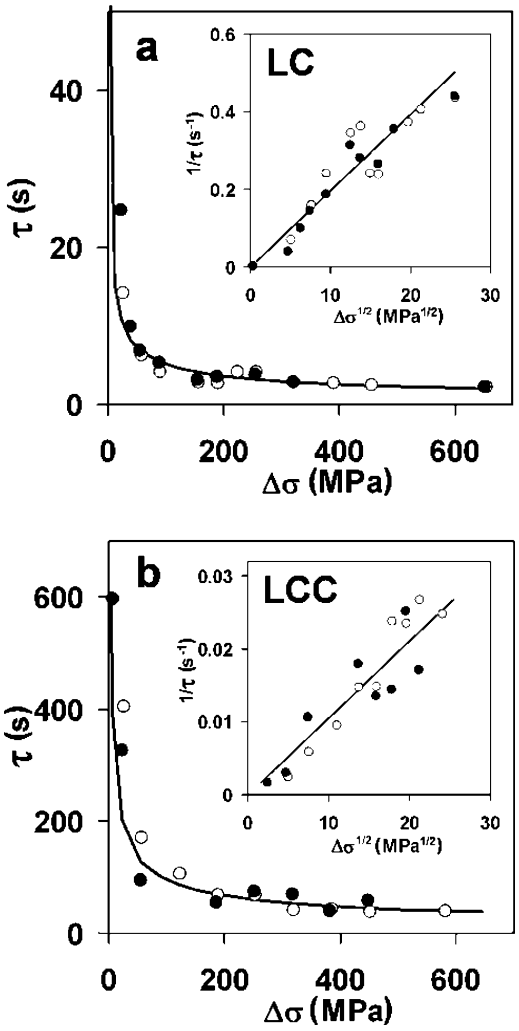

FIG. 9. Dependence of the characteristic time on switching stress increment: (a) LC (b) LCC. The insets show the $1/\tau$ versus $\Delta\sigma^{1/2}$. A linear dependence on such plots demonstrates the validity of Eq. (7).

$$\Delta\sigma = |\sigma - \sigma_{\text{ini}}|,$$

where σ is the applied stress, σ_{ini} is the initial stress that is the stress approaching zero for loading and the stress when unloading starts for unloading. The parameter $\Delta\sigma$ is always positive. The larger the switching stress increment, the higher the switching rate is, which is valid for both loading and unloading.

The dependence of the characteristic time τ on the switching stress increment $\Delta\sigma$ is shown in Fig. 9. To determine ε_{eq} and τ for a given applied stress, a fitting of the calculated [Eq. (5)] and corresponding experimental data of the creep strain ε_c was performed with the goal to maximize the R^2 parameter. First, the initial approximations for ε_{eq} and τ were determined using any two experimental points from the experimental creep (recovery) strain-time curve and finding the solutions by solving the system of two equations based on Eq. (5). The next approximations of ε_{eq} and τ were selected in the way which allowed the dependence ε_c as a function of t, calculated by Eq. (5), to be obtained maximizing the R^2 parameter. Therefore, the best estimate of ε_{eq} and τ was found. The errors in the determining τ were estimated as 1–2 s for LC and 15–20 s for LCC. As one can see from Fig. 9 both LC and LCC perovskites have a similar dependence of $\tau(\Delta\sigma)$ during loading and unloading. A good approximation of this dependence can be expressed as

$$\tau = \frac{A}{\Delta\sigma^{1/2}}, \tag{7}$$

where A is the numerical coefficient. Using Eq. (7) and following parameters, $\sigma_{\text{ini}}=8$ MPa for loading, $\sigma_{\text{ini}}=652$ MPa for unloading and $A=51$ s·MPa$^{0.5}$ for LC, and $\sigma_{\text{ini}}=8$ MPa for loading, $\sigma_{\text{ini}}=645$ MPa for unloading and $A=950$ s·MPa$^{0.5}$ for LCC, the characteristic time was calculated (solid lines in Fig. 9). The insets in Fig. 9 show a nearly linear dependence of $1/\tau$ versus $\Delta\sigma^{1/2}$ data, which demonstrates the validity of Eq. (7). Thus, the calculated values are in sufficient agreement with the characteristic time values obtained using experimental results.

F. Equilibrium stress-strain diagram

Stress-strain diagrams for LC and LCC perovskites are shown in Fig. 10. Solid lines correspond to the data measured in compression at a loading rate of 3 MPa/s (nonequilibrium diagram) and open circles correspond to the equilibrium strain values, where equilibrium strain ε_{eq} has been calculated using (5) and could be obtained at infinitely slow loading/unloading. As one can see from Fig. 10(a), for the LC perovskite the equilibrium stress-strain diagram almost coincides with the nonequilibrium one (the hysteresis areas are 0.271 MPa and 0.314 MPa, respectively) because of the fast switching and, as a result, a very small equilibrium strain increment $\Delta\varepsilon_{\text{eq}}$ ($\sim 10^{-5}$). What is also important to note is that at higher stress levels above ~200 MPa, the equilibrium strain values are almost coincident for the loading and the unloading portions of the deformation curves, meaning no hysteresis occurs above 200 MPa for the equilibrium stress-strain diagram.

For the LCC oxide the equilibrium strain increment $\Delta\varepsilon_{\text{eq}}$ is much larger ($\sim 10^{-4}$), which results in a significant difference between the equilibrium and nonequilibrium stress-strain diagrams. In the loading portion of the equilibrium diagram, the larger time-dependent ferroelastic strain of the sample is evident, i.e., the same stress results in larger strain when compared to the nonequilibrium diagram. There is also larger recovery in the equilibrium diagram as compared to the nonequilibrium deformation upon unloading. The hysteresis area is 0.563 MPa for the deformation under equilibrium conditions, and 0.853 MPa for the nonequilibrium stress-strain diagram. As in the case of equilibrium deformation of LC, no hysteresis is present above certain stress level (~300 MPa) for LCC oxide.

IV. CONCLUSIONS

The room-temperature creep and recovery processes in ferroelastic materials are essentially different from that occurring in materials at high temperatures. The creep mecha-

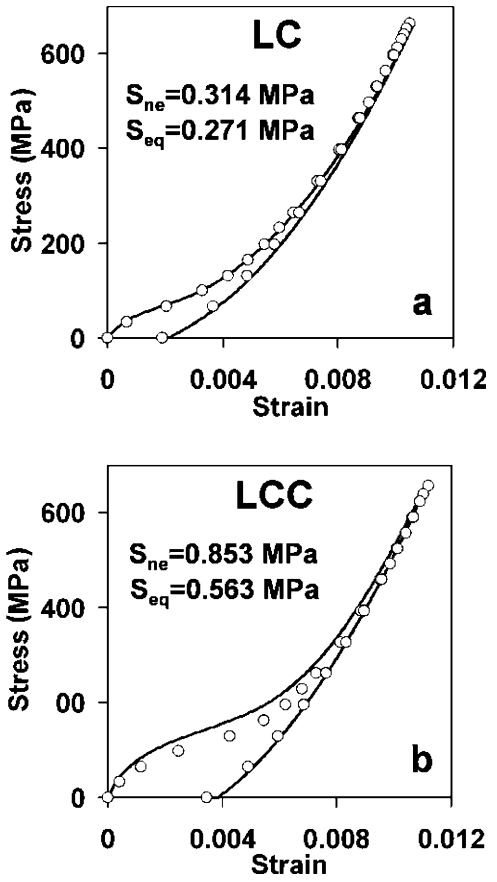

FIG. 10. Stress-strain diagrams for LC (a) and LCC (b). Open circles correspond to equilibrium strain values, a solid curve is a nonequilibrium diagram at a loading rate of 3 MPa/s. The S_{ne} and S_{eq} are hysteresis areas for nonequilibrium and equilibrium diagrams, respectively.

nism for ferroelastic materials, ferroelastic domain switching, is locally consumable leading to the existence/appearance of an equilibrium strain. Since only a finite number of domains are available to switch, the finite equilibrium strain will result after infinite holding time at constant stress.

A phenomenological model of the ferroelastic creep is proposed instead of the previously used power law. The model takes into account the existence of the equilibrium strain ε_{eq} and allows its estimation for a given stress level, while such an estimation is impossible using a power law. The proposed model provides high accuracy for prediction of the time-dependent creep properties especially for long term experiments lasting for several days.

Switching stress increment $\Delta\sigma$ is defined both for the loading and the unloading, and a phenomenological expression is developed to calculate a characteristic time from the increment. The characteristic time τ is a parameter that allows the measurement of the rate of the saturation/equilibrium of the creep (recovery) strain at a given applied stress.

The equilibrium stress-strain diagrams for LC and LCC oxides are calculated, and differences between equilibrium and nonequilibrium deformation diagrams are estimated. It is found that the hysteresis area under equilibrium and nonequilibrium deformation are nearly coincident for LC oxide because of the fast switching of the domains, while in LCC oxide, a larger creep strain and characteristic time of the material under equilibrium conditions was found, resulting in the larger strain and smaller hysteresis area when compared to the nonequilibrium deformation.

ACKNOWLEDGMENTS

The financial support of the National Science Foundation, USA through Grant No. DMR-0201770, the Royal Society, U.K. through Incoming Short Visit 2005/R3 scheme and European Commission through "Marie Curie Incoming Fellowships (IIF)" Grant No. 022066 of the 6th Framework Programme on Research, Technological Development and Demonstration is acknowledged.

[1] H. U. Anderson, Solid State Ionics **52**, 33 (1992).
[2] N.-L. Wu, W.-R. Liu, and S.-J. Su, Electrochim. Acta **48**, 1567 (2003).
[3] O. Haas, F. Holzer, S. Muller, J. M. McBreen, X. Q. Yang, X. Sun, and M. Balasubramanian, Electrochim. Acta **47**, 3211 (2002).
[4] M. Bursell, M. Pirjamali, and Y. Kiros, Electrochim. Acta **47**, 1651 (2002).
[5] V. Hermann, D. Dutriat, S. Muller, and Ch. Comninellis, Electrochim. Acta **46**, 365 (2000).
[6] R. Tan and Y. Zhu, Appl. Catal., B **58**, 61 (2005).
[7] N. A. Merino, B. P. Barbero, P. Grange, and L. E. Cadus, J. Catal. **231**, 232 (2005).
[8] S. Royer, D. Duprez, and S. Kaliaguine, J. Catal. **234**, 364 (2005).
[9] S. R. Sehlin, H. U. Anderson, and D. M. Sparlin, Phys. Rev. B **52**, 11681 (1995).
[10] L. Simonot, F. Garin, and G. Maire, Appl. Catal., B **11**, 167 (1997).
[11] M. S. D. Read, M. Saiful Islam, G. Watson, F. King, and F. E. Hancock, J. Mater. Chem. **10**, 2298 (2000).
[12] V. V. Kharton, F. M. Figueiredo, A. V. Kovalevsky, A. P. Viskup, E. N. Naumovich, A. A. Yaremchenko, I. A. Bashmakov, and F. M. B. Marques, J. Eur. Ceram. Soc. **21**, 2301 (2001).
[13] N. Orlovskaya, H. Anderson, M. Brodnikovskyy, M. Lugovy, and M. J. Reece, J. Appl. Phys. **100**, 026102 (2006).
[14] N. Orlovskaya, Y. Gogotsi, M. Reece, B. Cheng, and I. Gibson, Acta Mater. **50**, 715 (2002).
[15] N. Orlovskaya, N. Browning, and A. Nicholls, Acta Mater. **51**, 5063 (2003).
[16] J. S. Forrester and E. H. Kisi, J. Eur. Ceram. Soc. **24**, 595 (2004).
[17] G. Majkic, L. Wheeler, and K. Salama, Acta Mater. **48**, 1907 (2000).

[18] K. Kleveland, A. Wereszczak, T. P. Kirkland, M.-A. Einarsrud, and T. Grande, J. Am. Ceram. Soc. **84**, 1822 (2001).
[19] A. R. De Arellano-Lopez, U. Balachandran, K. C. Goretta, B. Ma, and J. L. Routbort, Acta Mater. **49**, 3109 (2001).
[20] T. Fett and G. Thun, J. Mater. Sci. Lett. **17**, 1929 (1998).
[21] D. Zhou and M. Kamlah, Acta Mater. **54**, 1389 (2006).
[22] M. W. Barsoum, *Fundamentals of Ceramics* (Institute of Physics, Bristol, 2003).
[23] S. C. Hwang and R. M. McMeeking, Int. J. Solids Struct. **36**, 1541 (1999).
[24] E. C. Subbarao, M. C. McQuarrie, and W. R. Buessem, J. Appl. Phys. **28**, 1194 (1957).
[25] O. Guillon, F. Thiebaud, P. Delobelle, and D. Perreux, J. Eur. Ceram. Soc. **24**, 2547 (2004).
[26] N. Orlovskaya, M. Lugovy, S. Pathak, D. Steinmetz, J. Lloyd, L. Fegely, M. Radovic, E. A. Payzant, E. Lara-Curzio, L. F. Allard, and J. Kuebler, J. Power Sources **182**, 230 (2008).